

# Wednesday 25 Nov

## PCB Manufacturing and Dimensional Measurement

Free webinar

14.00-16.00 CET | 08.00-10.00 EST

[Register here](#)



Uwe Brand  
Federal Institute of  
Physics & Technology,  
Braunschweig



Markus Fabich,  
Strategic Marketing  
Manager, Olympus



Wiley Analytical Science

**OLYMPUS**



# Hybrid Spintronic Materials from Conducting Polymers with Molecular Quantum Bits

Michal Kern, Lorenzo Tesi, David Neusser, Nadine Rufßegger, Mario Winkler, Alexander Allgaier, Yannic M. Gross, Stefan Bechler, Hannes S. Funk, Li-Te Chang, Jörg Schulze, Sabine Ludwigs, and Joris van Slageren\*

Hybrid materials consisting of organic semiconductors and molecular quantum bits promise to provide a novel platform for quantum spintronic applications. However, investigations of such materials, elucidating both the electrical and quantum dynamical properties of the same material have never been reported. Here the preparation of hybrid materials consisting of conducting polymers and molecular quantum bits is reported. Organic field-effect transistor measurements demonstrate that the favorable electrical properties are preserved in the presence of the qubits. Chemical doping introduces charge carriers into the material, and variable-temperature charge transport measurements reveal the existence of mobile charge carriers at temperatures as low as 15 K. Importantly, quantum coherence of the qubit is shown to be preserved up to temperatures of at least 30 K, that is, in the presence of mobile charge carriers. These results pave the way for employing such hybrid materials in novel molecular quantum spintronic architectures.

## 1. Introduction

Quantum sensing aims to enhance the sensitivity of sensing (electric or magnetic) fields or specific analytes.<sup>[1]</sup> Such applications typically require ambient or even physiological condi-

tions.<sup>[2]</sup> As with all quantum technologies, the basic functional unit is the quantum bit or qubit. Quantum bits are two- or more-level systems that can be prepared in coherent superposition states of these levels. Very often, electron spins are used to encode the quantum bit, because the lifetime (coherence time) of the superposition states can be rather long. Spin qubits based on paramagnetic molecules can be expected to make a positive contribution in this area, and, in fact, the quantum properties of spin labels have long been used to determine protein structures under ambient conditions.<sup>[3]</sup> In addition, the chemical tailorability of molecules may be exploited to enhance the chemical selectivity of quantum sensors, by integration of appropriate receptor functionalities.

An important figure of merit for potential qubits is the phase memory or quantum coherence time. Compounds proposed as molecular qubits (MQBs) have been shown to possess quantum coherence times of the order of hundreds of microseconds at low temperatures,<sup>[4–6]</sup> and up to microseconds at room temperature.<sup>[5,7,8]</sup> However, these measurements were all performed by electron paramagnetic resonance (EPR) techniques on bulk solid-state or (frozen) solution samples. Such techniques are based on the detection of microwave photons, which is inherently insensitive, due to the limited energy content of a microwave photon. At the moment, this precludes using MQBs in quantum devices. Techniques based on conversion of the quantum state of the qubit to a visible-light photon (optically detected magnetic resonance),<sup>[9–11]</sup> or techniques based on the addressing and readout of qubits via electrical currents<sup>[12–14]</sup> are more sensitive and, in principle, allow for single-qubit detection. Electrical readout has the advantage that the quantum sensor can be easily integrated with external control electronics that can process and amplify the electrical currents, and we, therefore, follow this approach here. In fact, electrical readout of MQBs has been shown to work, even at single-molecule level, but only at millikelvin temperatures.<sup>[13]</sup> For purposes of quantum sensing of analytes, millikelvin temperatures are not suitable, and higher temperature operation is essential. A successful system for electrical addressing of quantum bits must therefore consist of three ingredients: First, it must feature a quantum bit, in our case a paramagnetic molecule with a single unpaired electron. The qubit is then encoded into the two spin orientations (up and down) of the electron spin. Second, the

M. Kern, Dr. L. Tesi, N. Rufßegger, M. Winkler, A. Allgaier, Prof. J. van Slageren

Institute of Physical Chemistry and Center for Integrated Quantum Science and Technology

University of Stuttgart

Pfaffenwaldring 55, 70569 Stuttgart, Germany

E-mail: slageren@ipc.uni-stuttgart.de

D. Neusser, Dr. Y. M. Gross, Prof. S. Ludwigs

IPOC-Functional Polymers

Institute of Polymer Chemistry and Center for Integrated Quantum Science and Technology

University of Stuttgart

Pfaffenwaldring 55, 70569 Stuttgart, Germany

Dr. S. Bechler, H. S. Funk, Dr. L.-T. Chang, Prof. J. Schulze

Institute of Semiconductor Engineering and Center for Integrated

Quantum Science and Technology

University of Stuttgart

Pfaffenwaldring 47, 70569 Stuttgart, Germany

 The ORCID identification number(s) for the author(s) of this article can be found under <https://doi.org/10.1002/adfm.202006882>.

© 2020 The Authors. Advanced Functional Materials published by Wiley-VCH GmbH. This is an open access article under the terms of the Creative Commons Attribution License, which permits use, distribution and reproduction in any medium, provided the original work is properly cited.

DOI: 10.1002/adfm.202006882

system or part of it must be able to conduct electricity. These two functionalities may or may not be combined into a single component of the material. Finally, there must be some interaction between the quantum bit and the electrical current. The strength of this interaction must be carefully tuned: if the interaction is too weak, addressing and readout is clearly not possible because the two properties are essentially independent. If the interaction is too strong, it may destroy the quantum coherence: In fact, it is well known from electron spin relaxation theory that fluctuating electric fields coming from charge motion, such as lattice vibrations or mobile charge carriers, can couple to the electron spin via spin-orbit coupling, and lead to decoherence.<sup>[15,16]</sup>

A number of different interaction mechanisms between qubit spins and charge carriers that enable electrical addressing have been reported in the literature: 1) Spin-dependent recombination of charge carriers weakly coupled to the qubit,<sup>[17]</sup> 2) Spin-dependent tunneling of charge carriers directly coupled to the qubit,<sup>[18,19]</sup> 3) Spin-dependent transport through a quantum dot weakly coupled to the qubit system,<sup>[20–22]</sup> and 4) Spin-dependent scattering of itinerant charge carriers on the qubit.<sup>[23]</sup> Mechanisms 2) and 3) are relevant only at very low temperatures, however, limiting their suitability for quantum sensing applications at ambient temperatures.

A number of different systems/material classes may be envisaged to achieve electrical addressing of MQBs. Relevant in this regard are recent investigations of molecular quantum bits in potentially semiconducting molecular materials. However, in these works, the conductivity properties were not studied.<sup>[5,24–26]</sup> In fact, a recent report indicated that the presence of mobile charge carriers dramatically decreases the coherence time of molecular quantum bits by more than a factor of ten in such systems, which suggested that the electrical readout of molecular quantum bits may remain elusive.<sup>[25]</sup> An alternative to these small-molecule systems is presented by hybrid materials consisting of conducting polymers for the conductivity functionality and MQBs for the quantum coherence. The advantage of this approach is that both components can be optimized separately, and that the resulting material is flexible and easily processable from solution. Conductivity can be induced by electric fields, for example by fabricating field-effect transistors, or by chemical doping. The readout mechanism is then based on spin-dependent recombination of charge carriers. Such recombination has been demonstrated even at room temperature,<sup>[27]</sup> but has yet to be used for molecular qubit readout. The use of conducting polymers for electronics or spintronics applications is a very active research field. It has been shown that charge carrier mobilities in polythiophenes, for example, may reach values of up to  $10^{-1} \text{ cm}^2 \text{ V}^{-1} \text{ s}^{-1}$  and conductivities  $>10^5 \text{ S cm}^{-1}$ .<sup>[28–30]</sup> Furthermore, charge carrier spin lifetimes up to  $10^{-4} \text{ s}$ , spin diffusion lengths of  $1.2 \mu\text{m}$ , as well as coherence times of up to  $10^{-6} \text{ s}$  have been reported for such polymers.<sup>[31,32]</sup> Electrically detected magnetic resonance (EDMR) can be used to study the charge transport mechanisms and spin physics in conducting polymers.<sup>[27,33,34]</sup> Interestingly, it was recently shown that the spin diffusion constant can be much larger than the charge diffusion constant.<sup>[35]</sup> This opens up new perspectives regarding qubit readout by spin currents rather than charge currents.

Here we present results for a hybrid material (Figure 1) consisting of the molecular quantum bit  $[\text{Cu}(\text{dbm})_2]$

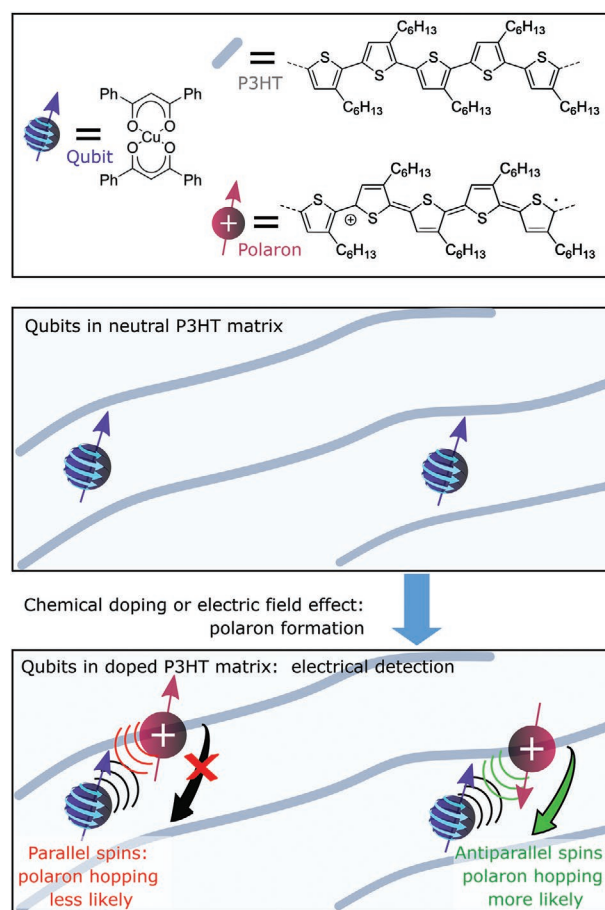


**Figure 1.** Schematic overview of the material studied and how this can potentially be used for electrical readout of MQBs. The top panel displays the components of the hybrid material: the molecular quantum bit  $[\text{Cu}(\text{dbm})_2]$  (Ph = phenyl, Hdbm = dibenzoylmethane), the polymer poly(3-hexylthiophene) (P3HT) and the chemical structure of the polaronic charge carrier in P3HT. In the absence of (polaronic) charge carriers (middle panel), electrical conductivity is low and no electrical readout is possible. In a field-effect transistor device, or by chemical doping, for example, by 2,3,5,6-tetrafluoro-tetracyanoquinodimethane ( $\text{F}_4\text{TCNQ}$ ), polaronic charge carriers can be introduced (bottom panel). The presence of MQBs and their spin orientations can be expected to influence the likelihood for spin-dependent charge transport processes in the conducting polymer, providing a mechanism for electrical detection of the qubit polarization.

(Hdbm = dibenzoylmethane), and the conducting polymer poly(3-hexylthiophene) (P3HT), where the latter is charge-doped with the electron acceptor 2,3,5,6-tetrafluoro-tetracyanoquinodimethane ( $\text{F}_4\text{TCNQ}$ ) to generate p-type charge carriers of polaronic and bipolaronic type. The rationale for our choice of materials combination is as follows: Some of us have previously studied the potential MQB  $[\text{Cu}(\text{dbm})_2]$  in detail and are therefore well-acquainted with its properties. It possesses rather long coherence times of up to  $47 \mu\text{s}$  in frozen  $\text{CS}_2$  solution and  $7.7 \mu\text{s}$  when doped into the corresponding, diamagnetic palladium(II) compound.<sup>[36]</sup> Furthermore, this neutral compound can be evaporated intact, underlining its chemical robustness, which is a clear advantage for surface deposition and addressing.<sup>[37]</sup> Similarly, P3HT is a very well-known conducting polymer that features good charge carrier

mobilities,<sup>[30,38]</sup> is commercially available, and well-studied by some of us.<sup>[38–40]</sup> The polaronic charge carriers in this p-type material at low doping levels are converted into bipolaronic charge carriers at higher doping levels. Typically, both charged species are delocalized over about five thiophene units.<sup>[41]</sup> In the present study, we generated charge carriers either by the field effect in field-effect transistor devices,<sup>[42]</sup> or by chemical doping with F<sub>4</sub>TCNQ.<sup>[43]</sup> We demonstrate that the charge transport is only a little affected by the presence of the MQBs. The polaronic charge transport processes were shown to be spin-dependent by EDMR experiments,<sup>[33]</sup> proving the principle viability of electrical readout out of the MQBs. We demonstrate that chemical doping, leading to the presence of mobile charge carriers in the material, has only limited effect on spin dynamics times. Demonstrating the survival of quantum coherence in the presence of mobile charge carriers is a first and essential step towards electrical readout of molecular quantum bits. Electrical addressing is required to achieve the necessary sensitivity and also for facile integration with control electronics. This firmly establishes hybrid materials of molecular quantum bits and organic semiconductors as a promising platform for development of quantum technological applications such as quantum sensors.

## 2. Results and Discussion

The paper is organized as follows. First, we describe the preparation and characterization of the thin films. The second part deals with the characterization of the conducting polymer thin films that incorporate the MQBs, establishing that the latter do not adversely affect the conducting properties of the polymers. MQBs often operate at temperatures below 100 K, and the low-temperature properties of the P3HT thin films are outlined in the third section, showing that in doped films, mobile charge carriers are present at temperatures as low as 15 K. In the final section, we discuss the quantum dynamics of the MQBs incorporated into (un)doped films, revealing sizable quantum coherence, even in the presence of mobile charge carriers.

### 2.1. Preparation and Characterization of Thin Films

We prepared thin films of P3HT by spin-coating under inert conditions. For the low-temperature EPR studies, spin-coated thin films proved to contain insufficient spins for reliable measurements, and we resorted to drop-casting for those studies. For both deposition methods, best results were achieved by using chlorobenzene as solvent and by preheating the solutions of P3HT and the poorly soluble [Cu(dbm)<sub>2</sub>] MQB to 70 °C before mixing, immediately followed by spin-coating. Doped P3HT films were prepared by means of established sequential doping procedures:<sup>[44,45]</sup> First, a P3HT film was deposited by spin-coating. Subsequently, the F<sub>4</sub>TCNQ dopant was deposited by spin-coating from an acetonitrile solution onto the freshly prepared undoped P3HT thin film. In the following, the resulting films are identified by the solution concentrations (in g L<sup>-1</sup>) of P3HT (P), [Cu(dbm)<sub>2</sub>] ([Cu]) and F<sub>4</sub>TCNQ dopant (D) before

spin-coating, for example, 12P/0.3[Cu]/1.3D for a film deposited by spin-coating from a solution of P3HT (12 g L<sup>-1</sup>) and [Cu(dbm)<sub>2</sub>] (0.3 g L<sup>-1</sup>) in chlorobenzene, with subsequent chemical doping by depositing the F<sub>4</sub>TCNQ dopant through spin-coating of a solution of F<sub>4</sub>TCNQ (1.3 g L<sup>-1</sup>) in acetonitrile. An en dash (–) denotes the absence of that particular component, for example, 12P/–/– for a P3HT film containing neither the [Cu(dbm)<sub>2</sub>] MQB, nor the F<sub>4</sub>TCNQ dopant. Figure S1, Supporting Information, displays AFM images of the films used for the room temperature current–voltage measurements. Film thicknesses were around 75 nm.

### 2.2. Room Temperature Characterization of Thin Film Samples

Figure 2a shows the UV/Vis/NIR spectra of P3HT thin films deposited by spin-coating from chlorobenzene solutions on glass substrates with different levels of post-deposition doping. The pristine film displays a clear absorption peak at about 18 000 cm<sup>-1</sup> (555 nm, 2.25 eV) attributed to the exciton

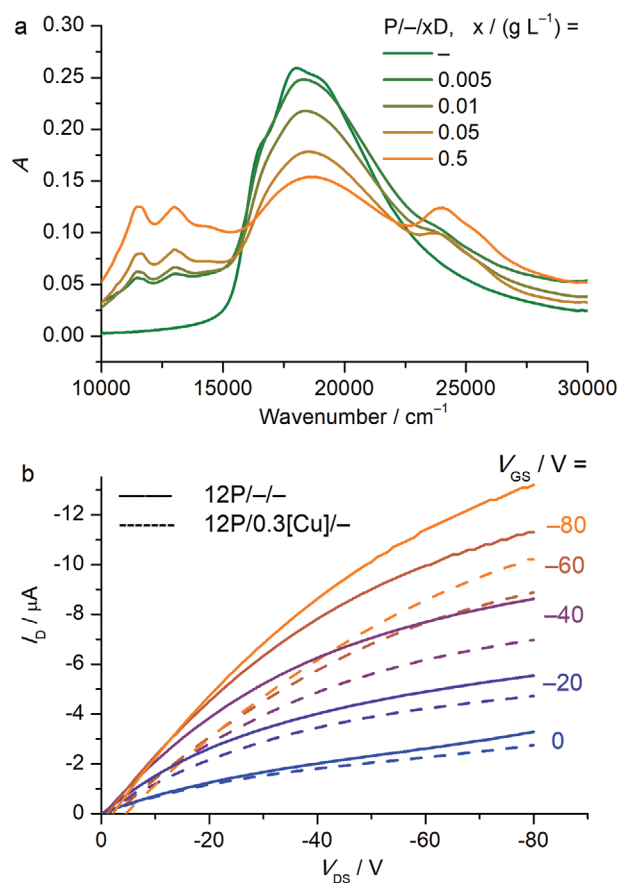


**Figure 2.** Room temperature characterization of thin films of P3HT (P), [Cu(dbm)<sub>2</sub>] ([Cu]) and F<sub>4</sub>TCNQ (D), where P, [Cu] and D concentrations (in g L<sup>-1</sup>) are given as P/[Cu]/D, prepared by spin-coating from chlorobenzene. a) UV/Vis spectra of thin films on glass slides with different doping concentrations of the F<sub>4</sub>TCNQ dopant (D) as indicated. b) Output characteristics of transistors based on 12P/–/– (solid lines) and 12P/0.3[Cu]/– (dashed lines) films deposited by spin-coating. The transistors had a channel length of 20 μm.

transition in P3HT. The presence of some vibronic fine-structure indicates a moderate degree of ordering in the film.<sup>[46]</sup> On doping, the intensity of the exciton band decreases and new bands at about  $13\,000\text{ cm}^{-1}$  (770 nm, 1.61 eV, highly structured) and about  $24\,000\text{ cm}^{-1}$  (417 nm, 2.98 eV) arise. The latter is attributed to the  $F_4TCNQ$  radical anion, while the former has been reported to be due to an intrapolaron electronic transition overlapping with a further  $F_4TCNQ$  transition.<sup>[46]</sup> These data show that the sequential doping procedure was successful. To assess the influence of the MQBs in the P3HT matrix on the latter's conductivity properties, we have carried out room-temperature current–voltage measurements on thin-film field-effect transistors based on P3HT films with and without MQBs. The transistors were fabricated by deposition of the components by means of spin-coating from chlorobenzene solutions onto silicon substrates in the inverted coplanar (bottom gate, bottom contact, Figure S2, Supporting Information) device architecture and had channel lengths between 2.5 and 20  $\mu\text{m}$ . The measured output characteristics (drain current versus drain-source voltage) for various gate-source voltages (Figure 2b and Figure S3–S5, Supporting Information) display a largely linear, Ohmic region at small drain-source voltages, and a saturation region at larger drain-source voltages, indicating complete development of the gate-field induced conduction channel. For the smallest channel length (2.5  $\mu\text{m}$ ), the contribution of the contact resistance to the total device resistance causes a pronounced nonlinearity at small drain-source voltages. At large drain-source voltages, the drain current does not saturate completely, that is, it still shows a weak dependence on the drain-source voltage, which we attribute to unintentional oxygen doping of the P3HT films.<sup>[47]</sup> The transfer characteristics (drain current versus gate-source voltage, Figure S6–S10, Supporting Information) indicate a large positive threshold voltage (approximately 20 V), potentially also a result of oxygen doping.<sup>[48]</sup> The effective charge-carrier mobility can be derived from the transfer characteristics as described in Section 3 of the Supporting Information.<sup>[32,49]</sup> The extracted effective carrier mobilities of  $\mu_{\text{sat}} = (0.5 \pm 0.1) \cdot 10^{-3}\text{ cm}^2\text{ V}^{-1}\text{ s}^{-1}$  for 12P/–/– and  $\mu_{\text{sat}} = (0.6 \pm 0.3) \cdot 10^{-3}\text{ cm}^2\text{ V}^{-1}\text{ s}^{-1}$  for 12P/0.3[Cu]/– show that the incorporation of the MQB into the P3HT matrix has no effect on the mobility within experimental error. The absolute values are typical for P3HT.<sup>[50]</sup> From complementary measurements on transistors with 3P/0.03[Cu]/– films prepared by spin-coating from chloroform (rather than chlorobenzene) solutions, a mobility of  $\mu_{\text{sat}} = (0.2 \pm 0.1) \cdot 10^{-3}\text{ cm}^2\text{ V}^{-1}\text{ s}^{-1}$  was extracted. This underlines that the electrical properties of the hybrid thin films are quite robust. Even higher mobilities can be obtained by specific crystallization techniques,<sup>[40,51]</sup> but this is not required for the present purposes.

In our experiments, the maximum number of spins in thin films prepared by spin-coating was of the order of  $10^{16}$  spins (Section 6 of Supporting Information), which is about double the detection limit of our EPR spectrometer. However, this required elevated [Cu] concentrations, for which the coherence time of the MQBs was determined to be very short,  $\approx 500\text{ ns}$  (see below). Hence, we resorted to drop-casting as an alternative sample preparation method, which allows us to prepare samples with higher absolute numbers of spins, but lower [Cu] concentrations (and therefore longer coherence times), due to

the increased film thickness. The effective carrier mobility of a transistor-based on 12P/0.6[Cu]/– deposited by drop-casting (Figure S11–S13, Supporting Information) was found to be  $\mu_{\text{sat}} = (1.9 \pm 0.9) \cdot 10^{-3}\text{ cm}^2\text{ V}^{-1}\text{ s}^{-1}$ , that is, slightly higher than the mobilities found for the spin-coated films. This can be expected, as slower drying processes involved in drop-casting compared to spin-coating generally improve the electrical performance of semiconducting polymers.<sup>[52–54]</sup>

### 2.3. Low-Temperature Charge Transport Properties of the Hybrid Thin Films

Quantum spin dynamics with measurably long timescales are usually associated with low temperatures, and we, therefore, studied the low-temperature charge transport properties of the hybrid P/[Cu]/D films prepared by drop-casting. Because low-temperature conductivities are expected to be very low, we performed the measurements on transistors with short channel lengths of 2.5  $\mu\text{m}$ . As a result, the quantitative results are more strongly affected by effects such as high contact resistance or high lateral electric fields compared to samples with channel lengths of hundreds of micrometers.<sup>[55]</sup> However, temperature-dependent trends are expected to be valid.

Figure S14, Supporting Information, shows the output characteristics of a transistor-based on 12P/0.3[Cu]/– deposited by drop-casting, measured at temperatures between 7 and 70 K. At these temperatures, the drain current is much smaller than at room temperature, and increases in a highly non-linear fashion with increasing drain-source voltage and without showing signs of saturation at high drain-source voltages. This non-linear behavior is caused by short-channel effects that are often more pronounced at lower temperatures, in part as a result of the temperature dependence of the contact resistance.<sup>[55]</sup> To investigate the influence of doping, we recorded the output characteristics of a transistor based on a 12P/0.3[Cu]/1.3D film deposited by drop-casting (Figure S15, Supporting Information), which were very similar to those of the transistor with the undoped semiconductor, with slightly higher leakage currents due to the higher conductivity of the doped semiconductor.

Because we will study the spin dynamics in the hybrid material in the absence of a gate-source voltage, we focused more in detail on the output characteristics of transistors based on doped and undoped P3HT, recorded at zero gate-source voltage (Figure 3). Under these conditions, the output characteristics are clearly different. For the undoped semiconductor (Figure 3a), the drain current is extremely small, and shows no systematic dependence on the applied drain-source voltage at temperatures below 60 K. In contrast, for the doped film (Figure 3b), the drain current is more than an order of magnitude larger and shows an approximately linear dependence on the drain-source voltage for all but the two lowest temperatures measured (7 and 10 K). These data demonstrate that in the doped films, mobile charge carriers are present at temperatures down to 15 K, even at zero gate-source voltage. In the absence of an Ohmic region in the output characteristics, the extraction of a reliable effective carrier mobility from these data is not possible. Therefore, instead of extracting an effective carrier

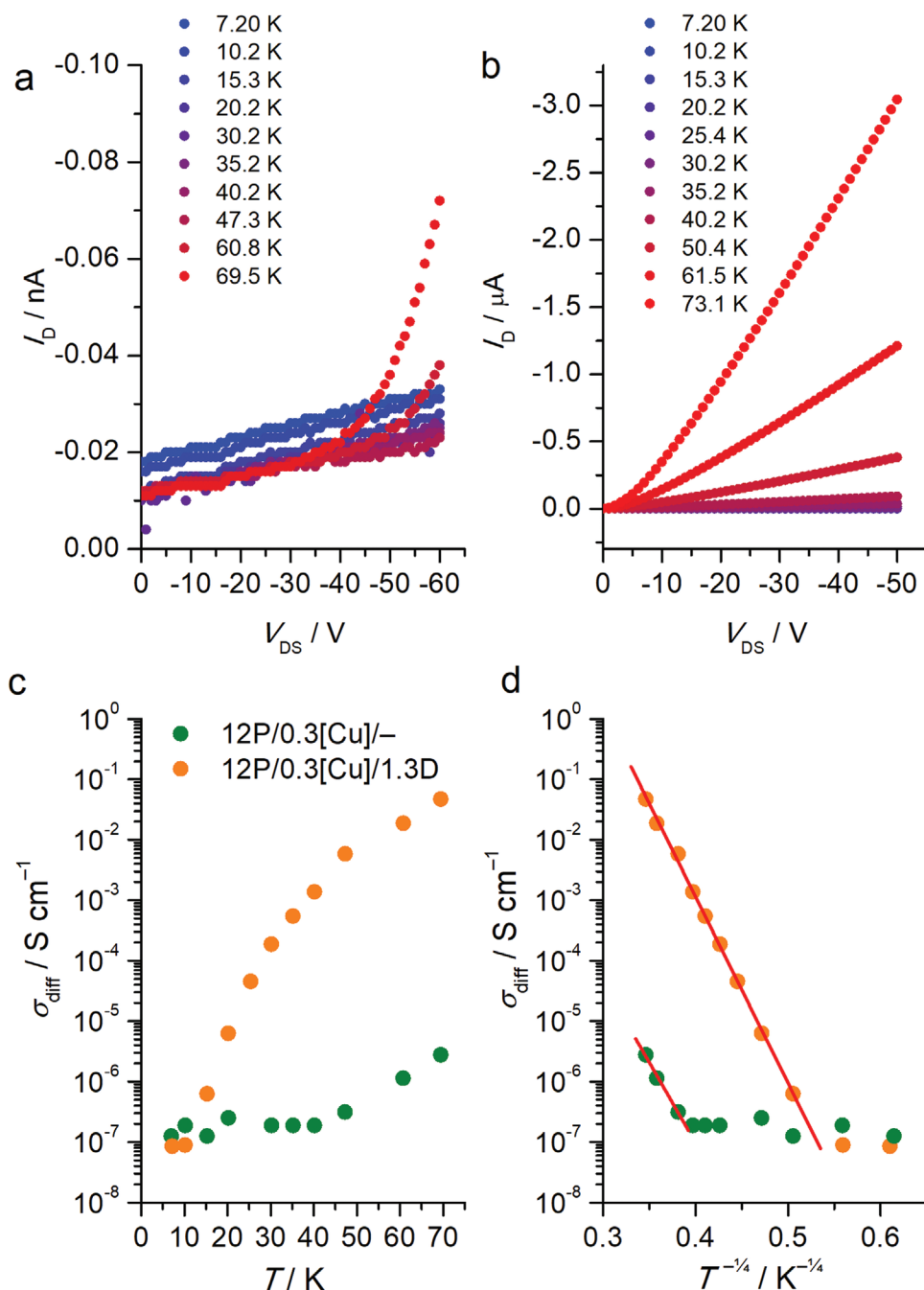


**Figure 3.** Variable temperature conductivity of P3HT films with [Cu(dbm)<sub>2</sub>] with and without F<sub>4</sub>TCNQ dopant. a) Output characteristics of a transistor-based on 12P/0.3[Cu]/-, deposited by drop-casting at various temperatures and at a gate-source voltage of zero. b) As a) for 12P/0.3[Cu]/1.3D. c) Differential conductivity measured by two-contact measurements on undoped and doped P3HT films deposited by drop-casting measured as a function of temperature. d) Same data as in c) plotted versus  $T^{-1/4}$ , including linear fits to the high-temperature region.

mobility, we have determined the differential conductivity  $\sigma_{diff}$  to assess charge-transport mechanisms and their temperature dependence (Figure 3c). The differential conductivity is given as the dependence of the drain current  $I_D$  on the drain-source voltage  $V_{DS}$  at the evaluation drain-source voltage  $V_{ev}$ :  $\sigma_{diff} = (\partial I_D / \partial V_{DS})_{V_{DS}=V_{ev}}$ . The differential conductivity at  $V_{ev} = -60$  V for the undoped sample is in the  $10^{-7}$   $S\ cm^{-1}$  range for essentially all temperatures, creeping up to  $10^{-6}$   $S\ cm^{-1}$  at

the highest temperatures. In contrast for the doped film,  $\sigma_{diff}$  ( $V_{ev} = -50$  V) strongly increases at temperatures above 10 K, with  $\sigma_{diff} > 10^{-2}$   $S\ cm^{-1}$  at 70 K. Figure 3d shows a clear linear dependence for the high-temperature region, when plotting  $\log \sigma_{diff}$  against  $T^{-1/4}$ . This observation suggests that the temperature-dependent contribution to the charge transport is governed by the Mott 3D variable-range-hopping mechanism, which predicts the differential conductivity to depend on temperature as

In  $\sigma_{\text{diff}} = \ln A - (B/T)^{1/4}$ .<sup>[56]</sup> Here  $A$  and  $B$  are arbitrary parameters. In order for electrical readout of quantum bits to work, the charge transport process must be spin-dependent. Only in that case, the current can be expected to depend on the quantum state of the molecular qubit. To demonstrate spin-dependent charge transport processes in our doped P3HT samples, we recorded EDMR spectra. In EDMR, the statistics of spin-dependent recombination processes are perturbed by microwave radiation. Figure S16, Supporting Information, displays an EDMR spectrum recorded at X-band frequencies (9.5 GHz) and room temperature. Because in EDMR, the current through the sample is recorded rather than microwave intensity, any signal must be due to mobile charge carriers, rather than the MQBs. The observation of a clear resonance line demonstrates therefore that charge transport in our doped P3HT samples features spin-dependent processes in agreement with published results on P3HT.<sup>[57]</sup>

## 2.4. Spin Dynamics of Hybrid Thin Films

As a first step in the study of the spin dynamics of the hybrid thin films, we have recorded the pulsed Q-band EPR echo intensity observed after a Hahn echo sequence ( $\pi/2-\pi$ -echo), as a function of external magnetic field  $B_0$ , yielding electron spin echo detected field-swept (ESE) spectra. For these measurements, we have used our recently developed Q-band Fabry–Pérot resonator that is optimized for flat samples such as the present thin films.<sup>[58]</sup> Figure 4a shows the ESE spectrum recorded at 7 K on a 6P/0.9[Cu]/– thin film deposited by spin-coating. The low-field part of the spectrum (1.07–1.23 T) is typical for a species with an axial  $g$ -tensor and is attributed to  $[\text{Cu}(\text{dbm})_2]$ , confirming the intactness of the MQBs in the polymer film. This part of the ESE spectrum was simulated, considering the spin Hamiltonian:

$$\hat{H} = \mu_B \vec{B}_0 \cdot \vec{g} \cdot \hat{S} + \vec{S} \cdot \vec{A} \cdot \hat{I} \quad (1)$$

Here  $\mu_B$  is the Bohr magneton,  $\vec{g}$  is the  $g$ -tensor,  $\vec{A}$  is the hyperfine tensor, and  $\vec{S}$  and  $\hat{I}$  are the electron and nuclear spin operators, respectively. The resulting parameters (Table 1) are essentially the same as those found for 0.001%  $[\text{Cu}(\text{dbm})_2]$  doped into  $[\text{Pd}(\text{dbm})_2]$ ,<sup>[36]</sup> denoted  $[\text{Cu}]_{\text{Pd}}$  in the following. At 1.2448 T, a small additional peak is observed ( $g = 2.0089$ ), which we assign to a radical species introduced by slight oxidation of the P3HT in agreement with the threshold voltage shift observed in the room-temperature transistor measurements (see above). We cannot be certain if these latter species are mobile polarons or stationary defects. The ESE spectrum recorded at 7 K on 12P/0.3[Cu]/– thin film deposited by drop-casting (Figure 4b) is very similar to that of the film deposited by spin-coating, but with slightly better signal-to-noise ratio due to the larger number of spins. The spectrum can be fitted with the same parameters as those of the spin-coated spectrum. Finally, we recorded the ESE spectrum of a doped 12P/0.3[Cu]/1.3D thin film deposited by drop-casting, also at a temperature of 7 K (Figure 4c). The low-field part, once again displays the peaks due to the [Cu] MQB, and can be fitted with the same spin Hamiltonian parameters. However, in contrast

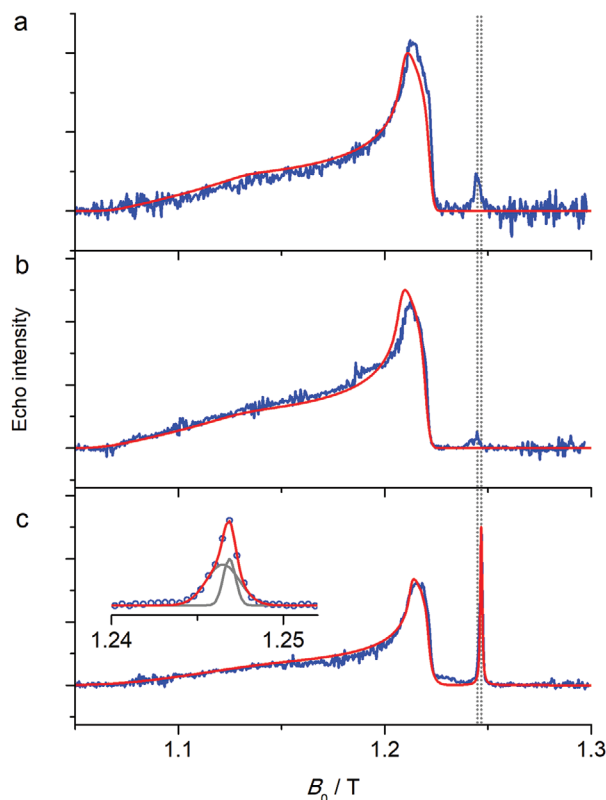


**Figure 4.** Electron spin echo detected field swept spectra recorded at 7 K on a) a 6P/0.9[Cu]/– thin film deposited by spin-coating, b) a 12P/0.3[Cu]/– thin film deposited by drop-casting, and c) a 12P/0.3[Cu]/1.3D thin film deposited by drop-casting. The inset of panel c) zooms in on the high-field peak revealing its compound nature.

to the previous spectra, this spectrum features an additional sharp resonance line at  $B_0 = 1.247$  T. Closer inspection (inset of Figure 4c) reveals that this sharp peak is asymmetric, possibly originating from two different species. These we attribute to the P3HT polaron (low-field component) and the  $F_4\text{TCNQ}$  radical anion (high-field component), respectively, on the basis of the higher  $g$ -value of the former.

We have determined the spin dynamics times of the [Cu] MQB for the 6P/0.9[Cu]/– film deposited by spin-coating, at the field position of the maximum in the ESE spectrum of Figure 4c. At 7 K, the spin–lattice relaxation time was determined by a monoexponential fit of the data (Figure S17, Supporting Information) to be  $T_1 = 4.5 \pm 0.3$  ms. This value is about a quarter of that found for  $[\text{Cu}]_{\text{Pd}}$ , which is surprisingly high: The spin–lattice relaxation time is related to the stiffness of the lattice,<sup>[5,59]</sup> and it appears that the P3HT lattice is not

**Table 1.** Spin Hamiltonian parameters obtained from fits of the ESE spectra of  $[\text{Cu}(\text{dbm})_2]$  in a 6P/0.9[Cu]/– thin film deposited by spin-coating ( $[\text{Cu}]_{\text{P3HT}}$ ), compared with 0.001%  $[\text{Cu}(\text{dbm})_2]$  in  $[\text{Pd}(\text{dbm})_2]$  ( $[\text{Cu}]_{\text{Pd}}$ )<sup>[36]</sup>.

Sample	$g_{\parallel}$	$g_{\perp}$	$A_{\parallel}$ [MHz]	$A_{\perp}$ [MHz]
$[\text{Cu}]_{\text{P3HT}}$	$2.27 \pm 0.02$	$2.056 \pm 0.002$	$550 \pm 30$	$80 \pm 10$
$[\text{Cu}]_{\text{Pd}}$	$2.255 \pm 0.005$	$2.050 \pm 0.001$	$570 \pm 10$	$78 \pm 10$

much less rigid than  $[\text{Pd}(\text{dbm})_2]$ , in spite of polymers belonging to so-called “soft matter”. This observation has an important implication in that  $T_1$  is the ultimate limit for the quantum coherence time, and it shows that polymeric matrices are eminently suitable for quantum technologies from that point of view. The spin-spin relaxation or phase memory time (which is a lower estimate of the quantum coherence time) was determined by Hahn echo measurements to be  $T_M = 0.78 \pm 0.02 \mu\text{s}$ . This phase memory time is much shorter than that reported for  $[\text{Cu}]_{\text{Pd}}$  (7.74  $\mu\text{s}$ ), which is due to the much larger spin concentration in the film deposited by spin-coating (15 wt%), leading to fast relaxation. The fast relaxation and weak signal intensity, the latter caused by a small absolute number of spins, precluded measurements above 13 K (Figure S17 and Table S2, Supporting Information). In fact, this was the main motivation to switch from spin-coating to drop-casting for film deposition (see above).

Hence, we investigated the spin dynamics of the undoped 12P/0.3[Cu]/– film deposited by drop-casting (Figure S18,S19; Table S3,S4, Supporting Information). First, spin–lattice relaxation curves turned out to be biexponential at low temperatures with a minor fast component. The major, slow component is reported in Table 2 and Figure 5. The spin–lattice relaxation time is again quite high at  $T_1 = 7.8 \pm 1.0 \text{ ms}$  at 7 K, decreasing rapidly with temperature, and reaching  $0.9 \pm 0.1 \mu\text{s}$  at 40 K. At higher temperatures, the relaxation time was too short to allow its reliable determination. This temperature dependence of  $T_1$  follows a power law  $T_1 \propto T^{-3.8}$ , which essentially parallels the behaviour of  $[\text{Cu}]_{\text{Pd}}$ ,<sup>[36]</sup> suggesting that a spin–lattice relaxation mechanism of the Raman kind is operative, which relies on molecular rather than lattice vibrations, as has been reported in literature for the related complex  $[\text{VO}(\text{dpm})_2]$  (Hdpm = dipivaloylmethane).<sup>[60]</sup> Second, we fitted the Hahn echo decay to a stretched exponential function  $I(2\tau) = I_0 \exp(-2\tau/T_M)^k$  to determine the phase memory time  $T_M$  of the undoped film (Figure S19, Supporting Information). Here  $I(2\tau)$  is the echo intensity at a time  $2\tau$  after the initial pulse,  $I(0)$  is the echo intensity at a delay time of  $2\tau = 0$ , and  $k$  is the stretch factor. At the lowest investigated temperature, 7 K, we found  $T_M = 3.84 \pm 0.02 \mu\text{s}$ , which is about half of the time found for  $[\text{Cu}]_{\text{Pd}}$ , but longer than for the film prepared by spin-coating, in line with the higher spin concentration in that film. Here it must be noted that the stretch factor  $k$  for the thin film sample was  $k = 1.51 \pm 0.02$  at 7 K and 1.00 at all other temperatures. In fact, we have previously observed that stretch factors different

**Table 2.** Spin dynamics ( $T_1$ ,  $T_M$ ) times, as a function of temperature for undoped 12P/0.3[Cu]/– and doped 12P/0.3[Cu]/1.3D films deposited by drop-casting.

$T$ [K]	$T_1$ (undoped) [ms]	$T_M$ (undoped) [ $\mu\text{s}$ ]	$T_1$ (doped) [ms]	$T_M$ doped [ $\mu\text{s}$ ]
7	$7.8 \pm 1.0$	$3.84 \pm 0.02$	$4.15 \pm 0.15$	$1.61 \pm 0.02$
10	$4.8 \pm 1.3$	$2.56 \pm 0.04$	$3.1 \pm 0.3$	$1.67 \pm 0.04$
15	$1.38 \pm 1.0$	$3.07 \pm 0.03$	$5 \pm 2$	$1.59 \pm 0.05$
20	$0.23 \pm 0.01$	$1.78 \pm 0.01$	$0.24 \pm 0.02$	$0.95 \pm 0.02$
30	$0.031 \pm 0.001$	$1.07 \pm 0.01$	$0.053 \pm 0.004$	$0.83 \pm 0.03$
40	$0.0009 \pm 0.0001$	$0.79 \pm 0.04$		

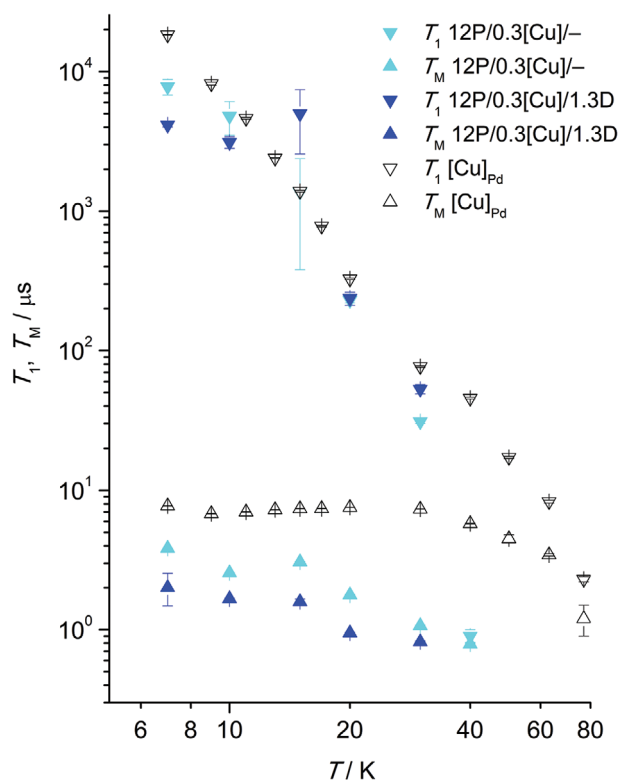


**Figure 5.**  $T_1$  and  $T_M$  times as a function of temperature, recorded on 12P/0.3[Cu]/– and 12P/0.3[Cu]/1.3D, both deposited by drop-casting. Hollow symbols are data for  $[\text{Cu}]_{\text{Pd}}$ , taken from.<sup>[36]</sup>

from 1 are found especially at low temperatures, and the decay curves become progressively more mono-exponential (i.e., the stretch factor becomes 1) at higher temperatures.<sup>[5,36,61]</sup> The stretch factor of  $k = 1.5$  suggests that at the lowest temperatures the physical movement of nuclear magnetic moment leading to spectral diffusion is the limiting factor to the phase memory time, but that at higher temperatures several decoherence mechanisms play a role. In contrast, for  $[\text{Cu}]_{\text{Pd}}$ , stretch factors  $k > 2$  were found for all temperatures below 40 K, indicating spectral diffusion by nuclear spin diffusion to be the relevant decoherence process.<sup>[36]</sup> The phase memory time decreases slowly with temperature and reaches  $0.79 \pm 0.04 \mu\text{s}$  at 40 K.

Finally, we investigated the doped, 12P/0.3[Cu]/1.3D film deposited by drop-casting (Figure S20,S21; Table S5,S6, Supporting Information), where transistor measurements revealed mobile charge carriers to be present at temperatures above 15 K (see above). Spin echoes could be observed at the lowest temperature, as for the film deposited by spin-coating. Gratifyingly, even at temperatures up to 30 K, spin echoes were found, demonstrating measurable quantum coherence at this temperature. From this, we can conclude that quantum coherence is largely preserved even in the presence of mobile charge carriers, in contrast to what had been observed previously.<sup>[25]</sup> In the dithiolate materials of ref. [25], electrical conductivity is engendered by suitable stacking of the dithiolate ligands in the solid, combined with charge doping. The quantum bit is prepared by one-electron oxidation of the gold complex, which can be viewed as molecular-level charge doping, and

the relevant orbital is largely localized on the dithiolate ligand. Thus, the same part of the sample is responsible for encoding the quantum bit as well as charge transport. It is possible that the intimate contact between the two functionalities strongly diminishes the quantum coherence. In contrast, in the P3HT/[Cu(dbm)<sub>2</sub>] material that we study, the charge transport is entirely along the P3HT part, that is, along the thiophene backbone combined with charge hopping between polymer chains. In contrast, the quantum bit is entirely localized on the copper(II)diketonate. Diketonates are not molecular semiconductors and thus play no role in charge transport. Thus, it is plausible that the spatial separation between the two functionalities leads to improved coherence properties. Spin–lattice relaxation times of the doped samples are slightly shorter than those for the undoped sample, but follow the same general trend (Figure 5). At the lowest temperature, the phase memory time is  $1.61 \pm 0.02 \mu\text{s}$  (Table 2) which is about half of that found for the undoped sample. At the highest temperature of 30 K, the phase memory time is still  $0.83 \pm 0.03 \mu\text{s}$ . For the doped sample, the Hahn echo decays turned out to be biexponential as has previously been observed for [Cu(dbm)<sub>2</sub>] in frozen solutions,<sup>[36]</sup> and is attributed to the complex residing in two different types of surroundings.

### 3. Conclusion

We have studied hybrid materials of the conducting polymer P3HT combined with the molecular quantum bit [Cu(dbm)<sub>2</sub>], both with and without the chemical doping agent F<sub>4</sub>TCNQ. Through careful and detailed investigations of both the charge transport and quantum spin dynamics properties, we have found that quantum coherence of the MQB is preserved, even at temperatures at which mobile charge carriers are present in the material. There is ample scope to further improve the properties of the material, such as to improve the electrical properties by post-processing, and to improve the coherence properties by deuteration. These results pave the way to addressing MQBs by means of electric currents and thus to using hybrid polymer/molecular qubit materials as a novel platform for quantum spintronics. Next steps will include tailoring and optimization of the material, the search for signatures of qubit-charge carrier interaction in transport measurements, and appropriate modeling to understand the interaction mechanism between the qubit and the charge carriers.

### 4. Experimental Section

**Materials:** Solvents were acquired commercially and used as received. Regioregular P3HT was bought from Merck and used without further purification. The number average molar mass extracted from gel permeation chromatography was  $\bar{M}_n = 28.7 \text{ kg mol}^{-1}$  with a polydispersity index of PDI = 1.77. F<sub>4</sub>TCNQ (>98.0%) was bought from TCI. [Cu(dbm)<sub>2</sub>] was prepared as previously.<sup>[36,62]</sup> For the fabrication of thin-film field-effect transistors, silicon substrates were purchased from Fraunhofer IPMS. Si substrates for EPR measurements with a size of  $15 \times 15 \text{ mm}^2$  were cut with a diamond saw from commercial lightly p-doped 4-inch wafers with specific resistivity of  $\rho = 1000 \Omega\text{-cm}$ . Commercial microscope slides were used as glass substrates for UV/Vis/NIR measurements.

**Semiconductor Film Preparation:** Substrates were cleaned 1) in an ultrasonic bath using acetone and isopropanol, 2) a CO<sub>2</sub> stream (Applied Surface Technologies Snowjet) with the substrate heated to 200 °C, and 3) an oxygen plasma (Diener electronic). Thin films were prepared inside the nitrogen atmosphere of a glove box. Films were deposited either by static spin-coating at 1000 rpm using a Süß MicroTec Delta-6RC spin-coater, starting from solutions of P3HT (12 g L<sup>-1</sup>) and [Cu(dbm)<sub>2</sub>] (1.8 g L<sup>-1</sup>), leading to film thicknesses of around 75 nm, or by drop-casting of a solution containing P3HT (24 g L<sup>-1</sup>) and [Cu(dbm)<sub>2</sub>] (2.6 g L<sup>-1</sup>) onto the substrate, with subsequent drying. The poor solubility of [Cu(dbm)<sub>2</sub>] in chlorobenzene was overcome by heating to 80 °C with continuous stirring. Chlorobenzene solutions of P3HT were pre-heated to 70 °C and mixed with the [Cu(dbm)<sub>2</sub>] solution immediately before film deposition. To generate p-type polaron charge carriers, a solution of F<sub>4</sub>TCNQ in acetonitrile was deposited onto the previously prepared P3HT film by spin-coating.

**Transistor Fabrication:** Thin-film transistors were fabricated in the bottom-contact, bottom-gate device architecture with a highly n-doped silicon substrate serving as a common gate electrode for all transistors on the substrates, and thermally grown silicon dioxide serving as the gate dielectric. Gold was used for the source and drain contacts. The transistors have channel lengths of 2.5, 5, 10, and 20 μm.

**Film Characterization:** Optical microscopy images were taken with a Zeiss Axio Imager microscope and AFM images were recorded with a Bruker Dimension Icon instrument in contact mode. AFM images were processed and analyzed using Gwyddion software.<sup>[63]</sup> UV/Vis/NIR spectra were recorded in the glovebox with a custom-built sample holder and a Zeiss MSC 621 VIS II spectrometer cassette.

**Charge-Transport Measurements:** Room temperature conductivity and transistor measurements were carried out inside the glove box, using a Süß MicroTec EP6 4-point probe station with a Keithley 2636B Source-Measure Unit. Low-temperature transport measurements were carried out on a home-built setup featuring a Keithley 2636B Source-Measure Unit and an Oxford Instruments Spectromag cryomagnet.

**Pulsed EPR measurements** were carried out using a home-built pulsed Q-Band (35.000 GHz) spectrometer, equipped with an Oxford Instruments CF9350 helium flow cryostat, and a home-built brass Fabry–Pérot resonator.<sup>[58,64]</sup> For the field-swept echo-detected spectra, the Hahn echo sequence was used with pulse lengths of 40 and 80 ns, as well as an interpulse delay of 300 ns. Easyspin was used for spectrum simulation.<sup>[65]</sup> The same sequence with varying interpulse delays was used for determining quantum coherence times. Spin–lattice relaxation times were determined by fast repetition or inversion recovery measurements. Saturation by fast repetition was used for undoped samples (both spin-coated and drop-cast) up to 15 K, and at higher temperatures inversion recovery was used. For doped samples, only inversion recovery was used. Equations S1–S3, Supporting Information, were used to fit the spin dynamics data.

**EDMR measurements** were carried out on a home-built spectrometer built around a modified Bruker EMX X-Band EPR spectrometer with a standard TE<sub>102</sub> rectangular cavity. MW radiation was supplied by an Anritsu MG3692C signal generator. The output power was set to 27.9 dBm. Constant bias voltage was applied to the sample by a five-piece stack of commercial 9 V batteries. Device current was pre-amplified by a FEMTO DLPCA-200 transimpedance amplifier and monitored with a Zürich Instruments MFLI lock-in amplifier. Field modulation was used to amplify the changes in device current due to magnetic resonance. Slightly p-doped Si (100) wafers with 200 nm of thermal SiO<sub>2</sub> on top, with custom interdigitated Ag electrodes ( $L = 2.5 \mu\text{m}$ ,  $w = 500 \mu\text{m}$ , see Figure S2, Supporting Information, for definition) deposited using photolithography and metal evaporation were used as substrate. P3HT layers (6 g L<sup>-1</sup>) doped with F<sub>4</sub>TCNQ (1.3 g L<sup>-1</sup>) were spin-coated onto pre-cut electrodes under inert conditions with the same procedure as described previously. After deposition, electrical contacts were made by soldering copper wires to the electrodes under ambient conditions (<15 min exposure). Contacted samples were then sealed in a custom sample holder with He gas atmosphere, which was directly inserted into the MW cavity.

## Supporting Information

Supporting Information is available from the Wiley Online Library or from the author.

## Acknowledgements

This work received financial support from the European Union's Horizon 2020 Research and Innovation Programme under Grant Agreement 767227 (FET-OPEN project PETER), the Center for Integrated Quantum Science and Technology (IQ<sup>ST</sup>), and the Carl Zeiss Foundation. The authors thank Benjamin Gerlach for experimental contributions at early stages of this work. The authors gratefully acknowledge useful discussions with James Borchert, Tobias Wollandt, and Dr. Hagen Klauk of the Max Planck Institute of Solid State Research in Stuttgart. The authors thank David Weißhaupt (IHT, University of Stuttgart) for cutting the transistor substrates.

Open access funding enabled and organized by Projekt DEAL.

## Conflict of Interest

The authors declare no conflict of interest.

## Keywords

charge transport, conducting polymers, molecular quantum bits, quantum coherence, thin film

Received: August 14, 2020

Revised: November 4, 2020

Published online:

- [1] C. L. Degen, F. Reinhard, P. Cappellaro, *Rev. Mod. Phys.* **2017**, *89*, 035002.
- [2] G. Balasubramanian, I. Y. Chan, R. Kolesov, M. Al-Hmoud, J. Tisler, C. Shin, C. Kim, A. Wojcik, P. R. Hemmer, A. Krueger, T. Hanke, A. Leitenstorfer, R. Bratschitsch, F. Jelezko, J. Wrachtrup, *Nature* **2008**, *455*, 648.
- [3] G. Y. Shevelev, O. A. Krumkacheva, A. A. Lomzov, A. A. Kuzhelev, O. Y. Rogozhnikova, D. V. Trukhin, T. I. Troitskaya, V. M. Tormyshev, M. V. Fedin, D. V. Pyshnyi, E. G. Bagryanskaya, *J. Am. Chem. Soc.* **2014**, *136*, 9874.
- [4] G. R. Eaton, S. S. Eaton, *J. Magn. Reson.* **1999**, *136*, 63.
- [5] K. Bader, D. Dengler, S. Lenz, B. Endeward, S.-D. Jiang, P. Neugebauer, J. van Slageren, *Nat. Commun.* **2014**, *5*, 5304.
- [6] J. M. Zadrozny, J. Niklas, O. G. Poluektov, D. E. Freedman, *ACS Cent. Sci.* **2015**, *1*, 488.
- [7] J. L. Du, G. R. Eaton, S. S. Eaton, *Appl. Magn. Reson.* **1994**, *6*, 373.
- [8] R. Owenius, G. R. Eaton, S. S. Eaton, *J. Magn. Reson.* **2005**, *172*, 168.
- [9] E. van Oort, N. B. Manson, M. Glasbeek, *J. Phys. C: Solid State Phys.* **1988**, *21*, 4385.
- [10] D. Suter, *Magn. Reson.* **2020**, *1*, 115.
- [11] S. L. Bayliss, D. W. Laorenza, P. J. Mintun, B. Diler, D. E. Freedman, D. D. Awschalom, *arXiv:quant-ph* **2020**, 2004.07998.
- [12] M. Niethammer, M. Widmann, T. Rendler, N. Morioka, Y.-C. Chen, R. Stöhr, J. U. Hassan, S. Onoda, T. Ohshima, S.-Y. Lee, A. Mukherjee, J. Isoya, N. T. Son, J. Wrachtrup, *Nat. Commun.* **2019**, *10*, 5569.
- [13] S. Thiele, F. Balestro, R. Ballou, S. Klyatskaya, M. Ruben, W. Wernsdorfer, *Science* **2014**, *344*, 1135.
- [14] J. Yoneda, K. Takeda, A. Noiri, T. Nakajima, S. Li, J. Kamioka, T. Kodera, S. Tarucha, *Nat. Commun.* **2020**, *11*, 1144.
- [15] A. Schweiger, G. Jeschke, *Principles of Pulse Electron Paramagnetic Resonance*, Oxford University Press, Oxford **2001**.
- [16] P. Huang, X. Hu, *Phys. Rev. B* **2014**, *89*, 195302.
- [17] A. R. Stegner, C. Boehme, H. Huebl, M. Stutzmann, K. Lips, M. S. Brandt, *Nat. Phys.* **2006**, *2*, 835.
- [18] M. H. Jo, J. E. Grose, K. Baheti, M. M. Deshmukh, J. J. Sokol, E. M. Rumberger, D. N. Hendrickson, J. R. Long, H. Park, D. C. Ralph, *Nano Lett.* **2006**, *6*, 2014.
- [19] S. Müllegger, S. Tebi, A. K. Das, W. Schöfberger, F. Faschinger, R. Koch, *Phys. Rev. Lett.* **2014**, *113*, 133001.
- [20] J. J. Pla, K. Y. Tan, J. P. Dehollain, W. H. Lim, J. J. L. Morton, F. A. Zwanenburg, D. N. Jamieson, A. S. Dzurak, A. Morello, *Nature* **2013**, *496*, 334.
- [21] R. Vincent, S. Klyatskaya, M. Ruben, W. Wernsdorfer, F. Balestro, *Nature* **2012**, *488*, 357.
- [22] M. Urdampilleta, S. Klyatskaya, M. Ruben, W. Wernsdorfer, *ACS Nano* **2015**, *9*, 4458.
- [23] A. Atxabal, M. Ribeiro, S. Parui, L. Urreta, E. Sagasta, X. Sun, R. Llopis, F. Casanova, L. E. Hueso, *Nat. Commun.* **2016**, *7*, 13751.
- [24] M. Warner, S. Din, I. S. Tupitsyn, G. W. Morley, A. M. Stoneham, J. A. Gardener, Z. Wu, A. J. Fisher, S. Heutz, C. W. M. Kay, G. Aeppli, *Nature* **2013**, *503*, 504.
- [25] J. McGuire, H. N. Miras, E. Richards, S. Sproules, *Chem. Sci.* **2019**, *10*, 1483.
- [26] M. Atzori, L. Tesi, E. Morra, M. Chiesa, L. Sorace, R. Sessoli, *J. Am. Chem. Soc.* **2016**, *138*, 2154.
- [27] H. Malissa, M. Kavand, D. P. Waters, K. J. van Schooten, P. L. Burn, Z. V. Vardeny, B. Saam, J. M. Lupton, C. Boehme, *Science* **2014**, *345*, 1487.
- [28] H. Sirringhaus, M. Bird, N. Zhao, *Adv. Mater.* **2010**, *22*, 3893.
- [29] V. Vijayakumar, Y. Zhong, V. Untilova, M. Bahri, L. Herrmann, L. Biniek, N. Leclerc, M. Brinkmann, *Adv. Energy Mater.* **2019**, *9*, 1900266.
- [30] *Conjugated Polymers: Properties, Processing, and Applications* (Eds: J. R. Reynolds, B. C. Thompson, T. A. Skotheim), CRC Press, Boca Raton, FL **2019**.
- [31] S.-J. Wang, D. Venkateshvaran, M. R. Mahani, U. Chopra, E. R. McNellis, R. Di Pietro, S. Schott, A. Wittmann, G. Schweicher, M. Cubukcu, K. Kang, R. Carey, T. J. Wagner, J. N. M. Siebrecht, D. P. G. H. Wong, I. E. Jacobs, R. O. Aboljadayel, A. Ionescu, S. A. Egorov, S. Mueller, O. Zadorna, P. Skalski, C. Jellett, M. Little, A. Marks, I. McCulloch, J. Wunderlich, J. Sinova, H. Sirringhaus, *Nat. Electron.* **2019**, *2*, 98.
- [32] S. Schott, U. Chopra, V. Lemaury, A. Melnyk, Y. Olivier, R. Di Pietro, I. Romanov, R. L. Carey, X. Jiao, C. Jellett, M. Little, A. Marks, C. R. McNeill, I. McCulloch, E. R. McNellis, D. Andrienko, D. Beljonne, J. Sinova, H. Sirringhaus, *Nat. Phys.* **2019**, *15*, 814.
- [33] C. Boehme, H. Malissa, *eMagRes* **2017**, *6*, 83.
- [34] C. Boehme, J. M. Lupton, *Nat. Nanotechnol.* **2013**, *8*, 612.
- [35] M. Groesbeck, H. Liu, M. Kavand, E. Lafalce, J. Wang, X. Pan, T. H. Tannahwa, H. Popli, H. Malissa, C. Boehme, Z. V. Vardeny, *Phys. Rev. Lett.* **2020**, *124*, 067702.
- [36] S. Lenz, K. Bader, H. Bamberger, J. van Slageren, *Chem. Commun.* **2017**, *53*, 4477.
- [37] F. Ciccullo, M. Glaser, M. S. Sättele, S. Lenz, P. Neugebauer, Y. Rechkemmer, J. van Slageren, M. B. Casu, *J. Mater. Chem. C* **2018**, *6*, 8028.
- [38] *P3HT Revisited – From Molecular Scale to Solar Cell Devices* (Ed: S. Ludwigs), Springer-Verlag, Berlin **2014**.
- [39] D. Neusser, C. Malacrida, M. Kern, Y. M. Gross, J. van Slageren, S. Ludwigs, *Chem. Mater.* **2020**, *32*, 6003.
- [40] E. J. W. Crossland, K. Tremel, F. Fischer, K. Rahimi, G. Reiter, U. Steiner, S. Ludwigs, *Adv. Mater.* **2012**, *24*, 839.

- [41] A. R. Chew, R. Ghosh, V. Pakhnyuk, J. Onorato, E. C. Davidson, R. A. Segalman, C. K. Luscombe, F. C. Spano, A. Salleo, *Adv. Funct. Mater.* **2018**, *28*, 1804142.
- [42] H. Klauk, *Chem. Soc. Rev.* **2010**, *39*, 2643.
- [43] K.-H. Yim, G. L. Whiting, C. E. Murphy, J. J. M. Halls, J. H. Burroughes, R. H. Friend, J.-S. Kim, *Adv. Mater.* **2008**, *20*, 3319.
- [44] I. E. Jacobs, A. J. Moulé, *Adv. Mater.* **2017**, *29*, 1703063.
- [45] D. T. Scholes, S. A. Hawks, P. Y. Yee, H. Wu, J. R. Lindemuth, S. H. Tolbert, B. J. Schwartz, *J. Phys. Chem. Lett.* **2015**, *6*, 4786.
- [46] D. T. Scholes, P. Y. Yee, J. R. Lindemuth, H. Kang, J. Onorato, R. Ghosh, C. K. Luscombe, F. C. Spano, S. H. Tolbert, B. J. Schwartz, *Adv. Funct. Mater.* **2017**, *27*, 1702654.
- [47] M. S. A. Abdou, F. P. Orfino, Y. Son, S. Holdcroft, *J. Am. Chem. Soc.* **1997**, *119*, 4518.
- [48] S. Brixi, O. A. Melville, N. T. Boileau, B. H. Lessard, *J. Mater. Chem. C* **2018**, *6*, 11972.
- [49] J. Zaumseil, H. Sirringhaus, *Chem. Rev.* **2007**, *107*, 1296.
- [50] R. Noriega, J. Rivnay, K. Vandewal, F. P. V. Koch, N. Stingelin, P. Smith, M. F. Toney, A. Salleo, *Nat. Mater.* **2013**, *12*, 1038.
- [51] K. Tremel, F. S. U. Fischer, N. Kayunkid, R. Di Pietro, R. Tkachov, A. Kiriy, D. Neher, S. Ludwigs, M. Brinkmann, *Adv. Energy Mater.* **2014**, *4*, 1301659.
- [52] K. Tremel, S. Ludwigs, in *P3HT Revisited – From Molecular Scale to Solar Cell Devices* (Ed: S. Ludwigs), Springer-Verlag, Berlin **2014**.
- [53] M. T. Dang, L. Hirsch, G. Wantz, J. D. Wuest, *Chem. Rev.* **2013**, *113*, 3734.
- [54] H. Yang, T. J. Shin, L. Yang, K. Cho, C. Y. Ryu, Z. Bao, *Adv. Funct. Mater.* **2005**, *15*, 671.
- [55] K. Tukagoshi, F. Fujimori, T. Minari, T. Miyadera, T. Hamano, *Appl. Phys. Lett.* **2007**, *91*, 113508.
- [56] N. F. Mott, E. A. Davis, *Electronic Processes in Non-Crystalline Materials*, Oxford University Press, Oxford **2012**.
- [57] K. Fukuda, N. Asakawa, *Macromol. Chem. Phys.* **2018**, *219*, 1700395.
- [58] S. Lenz, B. Kern, M. Schneider, J. van Slageren, *Chem. Commun.* **2019**, *55*, 7163.
- [59] M. Atzori, L. Tesi, S. Benci, A. Lunghi, R. Righini, A. Taschin, R. Torre, L. Sorace, R. Sessoli, *J. Am. Chem. Soc.* **2017**, *139*, 4338.
- [60] L. Tesi, E. Lucaccini, I. Cimatti, M. Perfetti, M. Mannini, M. Atzori, E. Morra, M. Chiesa, A. Caneschi, L. Sorace, R. Sessoli, *Chem. Sci.* **2016**, *7*, 2074.
- [61] S. Lenz, H. Bamberger, P. P. Hallmen, Y. Thiebes, S. Otto, K. Heinze, J. van Slageren, *Phys. Chem. Chem. Phys.* **2019**, *21*, 6976.
- [62] B.-Q. Ma, S. Gao, Z.-M. Wang, C.-S. Liao, C.-H. Yan, G.-X. Xu, *J. Chem. Crystallogr.* **1999**, *29*, 793.
- [63] N. David, K. Petr, *Open Phys.* **2012**, *10*, 181.
- [64] I. Tkach, A. Baldansuren, E. Kalabukhova, S. Lukin, A. Sitnikov, A. Tsvir, M. Ischenko, Y. Rosentzweig, E. Roduner, *Appl. Magn. Reson.* **2008**, *35*, 95.
- [65] S. Stoll, A. Schweiger, *J. Magn. Reson.* **2006**, *178*, 42.